Electronic Supplementary Material (ESI) for Physical Chemistry Chemical Physics.

SUPPORTING INFORMATION

Probing of Chain Conformations in Conjugated Polymer Nanoparticles by Electron Spin Resonance Spectroscopy

Christian Hintze‡, Friederike Schütze‡, Malte Drescher,* and Stefan Mecking*

CONTENTS

GENERAL METHODS AND MATERIALS

Particle sizes were determined by dynamic light scattering (DLS) with a Zetasizer Nano ZS (Malvern Instruments; 173° back scattering). The autocorrelation function was analyzed using the Malvern dispersion technology software 5.1 algorithm to obtain volume weighted particle size distributions, and polydispersitiescon. Transmission electron microscopy (TEM) was performed with a Zeiss Libra 120 EF-TEM instrument. Samples were prepared by application of a drop of aqueous particle dispersion to a carbon-coated grid and evaporation of water. Staining of the samples was conducted by addition of 2 µL of 1 % PTA in water to 100 µL of dispersion. NMR spectra were recorded on a Varian Unity INOVA 400 instrument. ^{1}H chemical shifts were referenced to the solvent signal. Multiplicities in ^{1}H NMR spectra are given in ppm as follows: s, singlet; t, triplet; m, multiplet. MALDI-TOF mass spectra were recorded using a Microflex mass spectrometer (Bruker Daltonics), equipped with a 335 nm nitrogen laser and operated in the linear mode. As a matrix, a saturated solution of α-hydroxycinnamic acid in a solution of 80 % acetonitril and 20 % water, with 0.1 % added trifluoracetic acid, was used. For sample preparation, 1 µL of the matrix solution was spotted on the MALDI target, dried, and 0.7 µL of the sample solution (10 µg/µL in chloroform) was added to the MALDI spot and dried again.

4-Carboxy-2,2,6,6-tetramethylpiperidine was purchased from Sigma Aldrich and was used without further purification. Tetrahydrofuran was distilled from sodium / benzophenone. All dispersions were prepared with Milli-Q-water.

The synthesis of monodisperse **HO-OPE$_n$-OH** (n = 5, 7, 9, 11, 21), **HO-OPE$_4$**, **HO-OPE$_{22}$** and **PEG-OPE$_9$** has been reported previously.[1]

ESR SPIN LABELED OLIGOMERS

Chemical structure of TEMPO labeled DL-OPE$_n$ oligomers

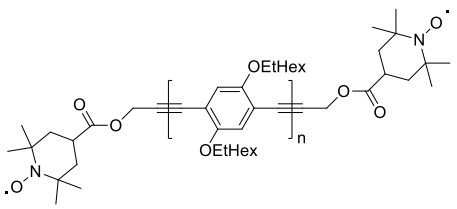

Figure S 1. Chemical structure of **DL-OPE$_n$**.

SL-OPE$_4$

^{1}H NMR (400 MHz, Chloroform-*d*) δ (ppm) 7.07 – 6.85 (m, 8H), 5.07 (s, 2H), 4.02 – 3.71 (m, 16H), 3.32 (s, 1H), 1.93 – 1.71 (m, 8H), 1.71 – 0.67 (m, 146H). **MALDI-TOF**: $m/z_{calc.}(C_{109}H_{164}NO_{11}) = 1664.2$; $m/z_{found} = 1650.3$;

DL-OPE$_5$

^{1}H NMR (600 MHz, Chloroform-*d*) δ (ppm) 7.03 – 6.95 (m, 8H), 6.92 (s, 2H), 5.08 (s, 4H), 3.96 – 3.81 (m, 20H), 1.87 – 1.73 (m, 10H), 1.69 – 0.69 (m, 174H). **MALDI-TOF**: $m/z_{calc.}(C_{144}H_{218}N_2O_{16}) = 2232.6$; $m/z_{found} = 2204.8$;

DL-OPE$_7$

^{1}H NMR (400 MHz, Chloroform-*d*) δ (ppm) 7.10 – 6.81 (m, 12H), 6.92 (s, 2H), 5.08 (s, 2H), 4.09 – 3.74 (m, 28H), 1.92 – 1.72 (m, 14H), 1.71 – 0.58 (m, 230H). **MALDI-TOF**: $m/z_{calc.}(C_{192}H_{290}N_2O_{20}) = 2946.2$; $m/z_{found} = 2918.4$;

DL-OPE$_9$

^{1}H NMR (400 MHz, Chloroform-*d*) δ (ppm) 7.37 – 7.00 (m, 18H), 5.30 (s, 4H), 4.34 – 3.93 (m, 36H), 2.20 – 1.98 (m, 18H), 1.98 – 1.38 (m, 144H), 1.37 – 0.84 (m, 108H). **MALDI-TOF**: $m/z_{calc.}(C_{240}H_{362}N_2O_{24}) = 3658.7$; $m/z_{found} = 3631.0$;

DL-OPE$_{11}$

^{1}H NMR (400 MHz, Chloroform-*d*) δ (ppm) 7.35 – 7.08 (m, 22H), 5.31 (s, 4H), 4.33 – 3.96 (m, 44H), 2.22 – 1.98 (m, 22H), 1.97 – 1.39 (m, 176H), 1.34 – 0.91 (m, 132H). **MALDI-TOF**: $m/z_{calc.}(C_{288}H_{434}N_2O_{28}) = 4372.3$; $m/z_{found} = 4344.5$;

DL-OPE$_{21}$

^{1}H NMR (400 MHz, Chloroform-*d*) δ (ppm) 7.06 – 6.90 (m, 42H), 5.05 (s, 4H), 3.99 – 3.79 (m, 84H), 1.88 – 1.74 (m, 42H), 1.72 – 1.18 (m, 336H), 1.05 – 0.82 (m, 252H). **MALDI-TOF**: $m/z_{calc.}(C_{528}H_{794}N_2O_{48}) = 7937.0$; $m/z_{found} \sim 7958$;

SL-OPE$_{22}$

^{1}H NMR (400 MHz, Chloroform-*d*) δ (ppm) 7.07 – 6.83 (m, 44H), 5.04 (s, 2H), 4.14 – 3.65 (m, 88H), 3.32 (s, 1H), 1.92 – 1.72 (m, 44H), 1.72 – 1.12 (m, 352H), 1.12 – 0.61 (m, 264H). **MALDI-TOF**: $m/z_{calc.}(C_{541}H_{812}NO_{47}) = 8081.1$; $m/z_{found} \sim 8084$;

MALDI-TOF MASS SPECTRA

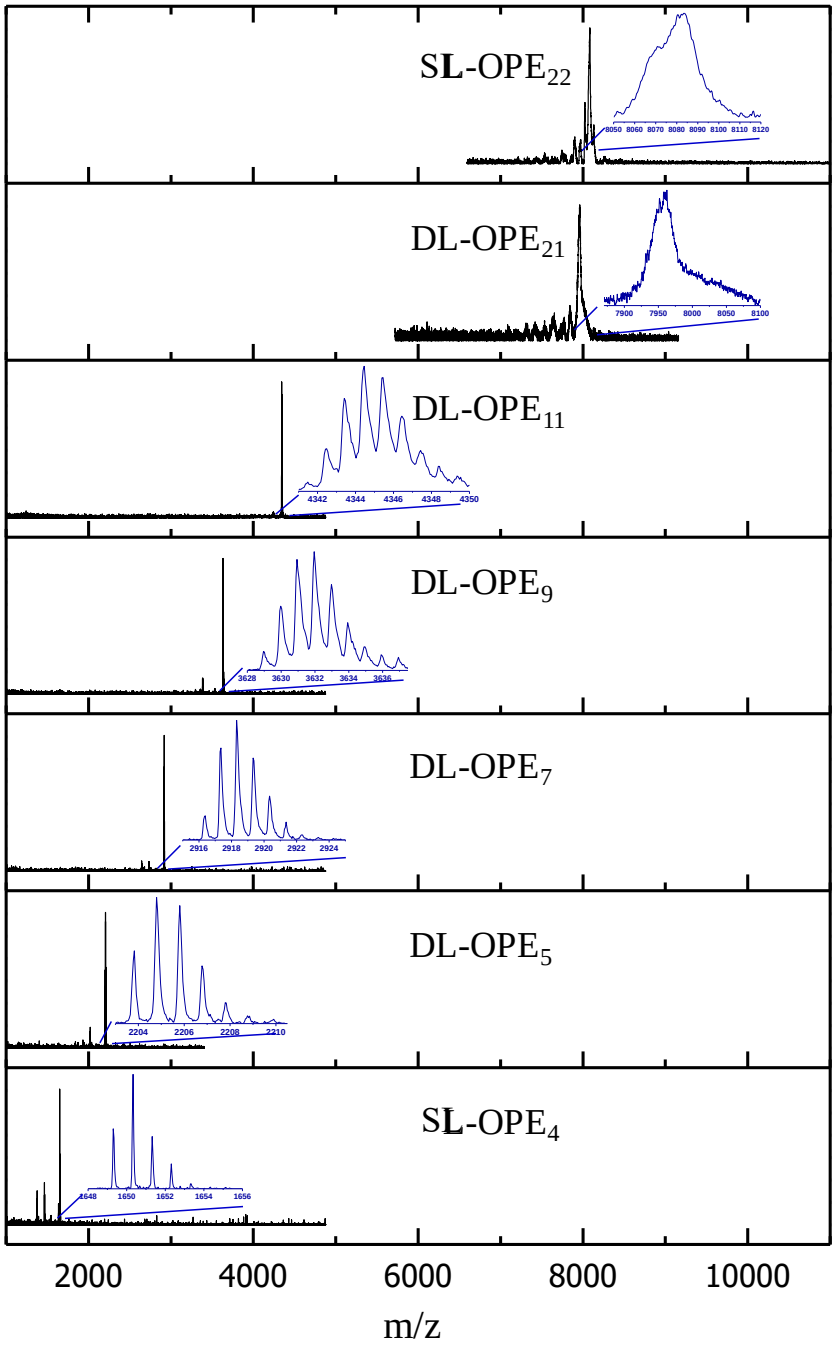

Figure S 2. MALDI-TOF mass spectra of doubly and singly labeled oligomers.

DETAILS ON BENDING ENERGY VS. SURFACE ENERGY

The enthalpy of the elongated state of an **OPE21** incorporated into a nanoparticle, where the chain sticks out of the nanoparticle core is dominated by its surface energy[2]. The free surface energy is a driving process for a solvated OPE-chain to cluster with other chains or incorporate into a micelle. Because single chains have a low volume to surface ratio, the free surface energy in this case is an enthalpically dominated driving force towards assembly[2] and is thus independent of temperature. It can be estimated by approximating the OPE-chain as a cylinder.

The length of this cylinder is given by the number of repeat units and the length of one such unit. In the case of an **OPE21** the length is given as $L_{21} = 21 * 0.69\ \text{nm} = 14.5\ \text{nm}$. Its diameter can be derived as follows. The benzene ring in the backbone has a width of 240 pm, obtained from the benzene bond length being 139 pm and simple trigonometry. The distance to the oxygens in the EtHexO-sidechains equals 121 pm (140 pm C-O bond length and simple trigonometry), adding another 242 pm. The radius of gyration of the EtHex chains was derived by using theoretical derivations made for dimensions of polymer chains with short-range interactions. One can look up the details in any polymer text book (e.g. Polymer Solutions by Teraoka[3]). The radius of gyration is given as $R_g^2 = {}^1/_3\, N\beta^2$, with β being the bond length and N, the number of bonds. For both EtHex sidechains together we assume β = 154 pm and N = 16. Here, the difference in bond length and angle for the carbon in the ether is neglected. In scope of the approximations made here, this should be not significant. This yields R_g = 356 pm. In total the diameter of the OPEs used in this work can be estimated to be α = 1.2 nm.

Thus, the corresponding cylinder has a surface area of A = 57 nm². The surface tension γ of the OPEs can be approximated by comparison with similar compounds. For Polystyrene it was found[4] to be γ = 40 mJ/m², which is nearly the same for several aliphatic hydrocarbons[5]. Since the OPE's surface should be dominated by the EtHex-sidechains, this should be a satisfying approximation. The surface energy for a single chain of **OPE21** amounts to roughly $H_{surf,max} = 1400\ \text{kJ/mol}$.

Since the surface energy is rather high, the chain might collapse in order to minimize surface area. While incorporated into a nanoparticle, it might still be stretched out inside the particle core and stick out of this sphere. In a particle core defined by the length of **OPE9**, twelve repeat units then would protrude out of the core. Hence, a sphere with the volume of these twelve repeat units would have the minimal solvated surface (21 nm²). In this case, the surface energy amounts to roughly $H_{surf} = 500\ \text{kJ/mol}$. The exact surface energy might be a little smaller, since the

surrounding near to the outer surface of the particle core is dominated by the PEG-chains and not only water.

Another possibility is not only avoiding chain bending, but also concomitant particle elongation. This would result in a cigar shaped particle in order to incorporate the elongated chain completely. We are thus interested in the change of surface from a sphere to a prolate spheroid retaining the volume. If b is the semi-major axis of the spheroid and equal to half of the chain length of **OPE21**, b = 7.3 nm, one can derive a, the semi-minor axis of the spheroid, with $V = \frac{4}{3}\pi\, a^2 b = \frac{4}{3}\pi\, R^3$. This yields $a = \sqrt{\frac{R^3}{b}} = 2.2$ nm for the optimum radius $R = R^* = 3.3$ nm (derived below). The surface area of such a spheroid is about 28 nm² larger than the corresponding sphere. The difference in surface energy between both cases is proportional to the difference between PPE-water surface tension γ and water-vapor surface tension[6] γ_w = 72 mJ/m²: $\Delta\gamma = \gamma_w - \gamma = 32$ mJ/m².[7] With this difference in surface tension and the aforementioned difference in surface area, we obtain an excess of surface energy of, again, $H_{surf,sph} = 500$ kJ/mol.

Restriction of conformational space of the oligomer chain gives rise to entropic cost involved with the incorporation into nanoparticles. The chain can be modelled as a harmonic segmented chain.[8,9] The segments for OPEs are the phenylene ring, the bond between a phenylene and an ethynylene ring, and the triple bond. The angle at the joint between two segments is determined by a harmonic bending potential. Since the chain rotated freely at its joints, in the unperturbed state there is no potential for the torsion angle. In this case, the entropy for a single joint is given to be $S_{unp} = \mathrm{R}\ \ln\Omega$, with R, the universal gas constant, and Ω, the number of microstates arising from the free rotation. When confined into the particle, rotation is restricted, consequently reducing the number of microstates. With the segments being small compared to the curvature of a sphere corresponding to the outer perimeter of the nanoparticle core, roughly half of the torsion angles are not accessible for the segments. The entropy for a single joint coinciding with the particle perimeter, which would be the most restricting case, thus is $S_{cnstr} \approx \mathrm{R}\ \ln\frac{\Omega}{2}$. Summing over all 84 joints of the **OPE21**, the change of entropy is

$$\Delta S \approx 84\ \mathrm{R}\left(\ln\left(\frac{\Omega}{2}\right) - \ln\Omega\right) \approx -84\ \mathrm{R}\ \ln 2.$$

Summarizing these contributions to the change of Gibbs energy we obtain at room temperature

$$\Delta G = \Delta H - T\Delta S = \left((7 - 500) + 144\right)\frac{\mathrm{kJ}}{\mathrm{mol}} = -350\,\frac{\mathrm{kJ}}{\mathrm{mol}}.$$

With the difference of Gibbs energy ΔG being negative by some hundreds of kJ/mol, chain bending into nanoparticles, where the particle diameter is smaller than the chain length, will be favorable.

OPTIMUM MICELLE SIZE

It remains unclear at this point, why the observed **PEG-OPE$_9$** particles are smaller when coprecipitated with **OPE$_{21}$**. To this end, a consideration of the expected micelle size of particles formed by **PEG-OPE$_9$** is instructive. With the assumption of a densely packed interior and a roughly spherical micelle, the micelle radius R is given by $\frac{4}{3}\pi R^3 = N\delta a^2$, with δ, the mean distance between the polar headgroup and any atom in the apolar part of the surfactant molecule, and N, the aggregation number. It can be shown[7], that the optimum aggregation number is given by $N^* = \frac{49\pi\gamma\delta^2}{48kT}$.

The average distance between the polar head and any atom in the apolar part within a coil-rod-coil polymer is approximately $\delta = \frac{L_n}{4}$ with $L_n = (0.69\ \text{nm})\ n$ and n, the number of repeat units of the **OPE$_n$** of interest. Thus, the optimum micelle radius for **PEG-OPE$_9$** can be expressed as

$$R^* = \frac{L_9}{4}\sqrt[3]{\frac{3}{4}\frac{49a^2\gamma}{48kT}}.$$

With the aforementioned surface tension the micelles are calculated to have an optimum diameter of D^* = 6.6 nm, which is close to the **OPE$_9$** contour length, L_9 = 6.1 nm. Since this is less than half of its persistence length L_p, the rigid **OPE$_9$** cannot arrange freely inside the particle core. Thus, the implicit assumption of a densely packed interior does not apply, the micelle radius being rather $\frac{4}{3}\pi R^3 = NL_9a^2$. In this case, incorporating **OPE$_{21}$** into the core of a particle constituted by **PEG-OPE$_9$** will be favorable. The contour length of **OPE$_{21}$** is approximately equal to the persistence length, $L_{21} \approx L_p$. This flexibility relative to the shorter **OPE$_9$**-fragments allows for an overall denser packing in the **OPE$_{21}$** containing particles.

SAMPLE PREPARATION FOR ESR

The ready-made particle samples were gathered into a 3 mm OD quartz glass tube upon freeze-drying. After collection, the voluminous solid particles were compressed by a factor of ~5-10 (volume). The compressed pellet of particles was then pushed out of the tube and collected into a

1 mm ID quartz tube, thereby compressing the sample another factor of ~5-10 (volume). Figure S 3 shows an example of one of the samples prepared that way.

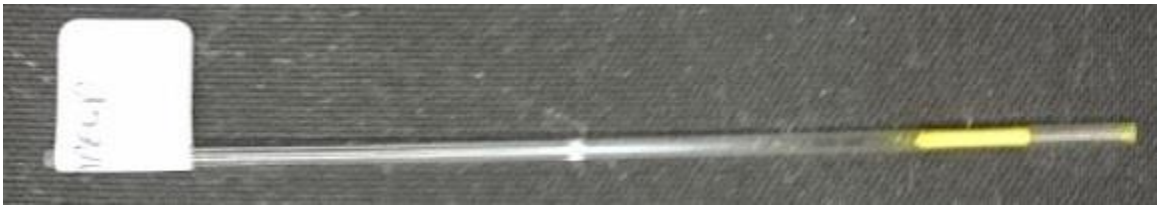

Figure S 3. Example of one of the samples prepared for the *in-particle* experiments.

ANALYSIS OF DEER DATA

Processing and distance distribution analysis of the DEER time trace was performed using the DeerAnalysis2013 software.[10] The zero time was determined automatically by built-in DeerAnalysis-routines to correct for $\tau \approx t - 120$ ns. The cutoff was optimized to avoid end artifacts due to overlap of excitation bandwidths. The background start was determined automatically by built-in DeerAnalysis-routines and was checked manually for the respective spin label concentrations (calibrated "Density" in DeerAnalysis). Afterwards, the distance distribution was extracted with model based fitting of the DEER time trace.

The data from samples with the probe in solution were analyzed with the worm like chain (WLC) model with Gaussian broadening accounting for label flexibility. The latter was determined as the average of the individual independent fits of all DEER time traces and subsequently kept constant for determination of the persistence lengths for the individual data sets.

The data from *in-particle* measurements on **DL-OPE$_{21}$** were analyzed with the model of a Rice distribution.[11] Additional correction for limited excitation bandwidth[12] was applied. The excitation bandwidth was estimated as an average of all excitation bandwidths of all pulses used in the DEER measurements. It was found to be 10 MHz in all cases.

ANALYSIS OF CW-ESR SPECTRA

Prior to the analysis of distance distributions, all spectra were corrected for their respective baseline with the help of Xepr, provided by Bruker Biospin. A script written in Matlab (Matlab R2015a) carried out all following steps necessary to extract distance information from the cw-ESR

spectra. First of all, the field swept spectra were converted into spectra in frequency space by relying on an approximate g-value obtained by the magnetic field value of the zero crossing of the central transition and the frequency given by the spectrometer software. Then, with the known frequency steps of the individual data points in the converted spectra, a series of Pake patterns have been computed within a frequency range between ± 10/2π GHz for a range of interspin distance from 0.8 … 8.0 nm. A Rice distribution with the help of the model script provided by DeerAnalysis was computed as well for the same range of distances. A cumulative Pake pattern for the according distance distribution was obtained by a weighted sum over the pre-computed Pake patterns, with the distance distribution itself providing the individual weights. An unbroadened reference spectrum (of a singly labeled probe in this case) was then convoluted with this cumulative Pake pattern and compared to the broadened spectrum shown in the main manuscript by means of root mean square deviations. For this purpose, the spectra were normalized to their maximum. Utilizing the built-in Matlab-function '`fmincon`', this RMSD has been minimized by variation of the parameters in the Rice distribution, yielding the best-fit parameters of the distance distribution of the cw-ESR spectrum of interest.

MODULATION DEPHTS OF *in-particle* MEASUREMENTS

Table S 1. Modulation depths of *in-particle* measurements presented in the main manuscript. They are usually about 8±3 % (normalized to pump-pulse lengths by simple approximation of the fraction of excited spins as the fraction between the pump-pulse length and the average pump-pulse length) due to reduction of the nitroxide spin labels used during the preparation of the particles.

Sample	Pump Pulse Length [ns]	Modulation Depth [%]	Norm. Mod. Depth [%]
DL-OPE$_5$ in **PEG-OPE$_9$**-a Particles	30	7	6
SL-OPE$_{22}$ in **PEG-OPE$_9$**-a Particles	40	11	13
DL-OPE$_{21}$ in **PEG-OPE$_9$**-a Particles	28	12	10
DL-OPE$_{21}$ in **PEG-OPE$_9$**-b Particles	34	5	5

DEER ON SL-OPE$_{22}$ IN PARTICLES – CONTROL SAMPLE

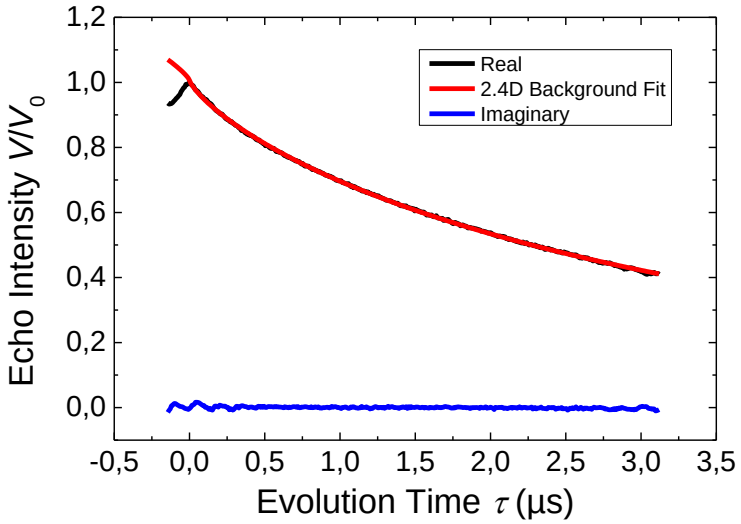

Figure S 4. Normalized DEER time trace recorded at 50 K in Q-band, with a 2.4 dimensional homogeneous background contribution of **SL-OPE$_{22}$** in particles with high **OPE$_{21}$**-content. The background was fitted to the experimental data starting at the zero time, thus deviating at negative times. No apparent dipolar oscillations occur, thus excluding the possibility of intermolecular contributions to the observed dipolar interactions reported.

HOMOGENEOUS BACKGROUND WITH REDUCED DIMENSIONALITY OR INTERMOLECULAR DISTANCE CONTRIBUTIONS?

Within the main manuscript it is stated, that intermolecular contributions to the *in-particle* DEER measurements were eliminated by exploiting a singly labeled probe, see also Figure S 4. More specifically, a 2.4D homogeneous background fit was used to evaluate the DEER data.

In this section, we would like to discuss this issue further. It might be hypothesized, that the observation of reduced dimensionality is actually not true. There might be another inhomogeneous intermolecular contribution, and that actually a 3.0D homogeneous background is present. Therefore, by applying the 2.4D homogeneous background correction like in the paper, this intermolecular distance contribution will be suppressed and the modulation depth would be reduced.

If more than one chain is incorporated in one nanoparticle, it would, on average over multiple such nanoparticles, look like spins randomly distributed on a spherical surface. Within the scope of this section, we want to look into this hypothetical inhomogeneous distance contribution. Others could be thought of as well, e.g. equal distribution of spins in a sphere, two chains building up a

supra-molecular unit with defined arrangement, etc. These other possibilities would be rather speculative and a spherical surface of spins seems to be the most probable one.

For this reason, we look again on all the data obtained from *in-particle* DEER measurements. They are analyzed again with the help of DeerAnalysis (see above), but this time by applying a 3.0D background correction instead of a 2.4D one. The results are shown in Figure S 5 and all parameters are given in Table S 2. It can be seen, that the reduced dimensionality of the background function might stem from additional inhomogeneous distance contributions. Namely, from inter-molecular interactions of spin labels of multiple chains, when more than one chain is included in the nanoparticle, giving rise to a distribution of spins on a sphere.[13] With a free fit of all parameters, a sphere diameter of around 6 nm is found in three out of four cases. We would like to note, that the parameters depend heavily on the choice of the background start and that the data presented by choosing the background start with best knowledge. Only in the case of **DL-OPE$_5$** almost no influence of the dimensionality of the background correction was found, yielding similar WLC distance distributions with 3.0D as well as with 2.4D background correction.

One could conclude that indeed the particle diameter actually present was measured as well in the DEER experiments, thus the 2.4D homogeneous background correction applied in the paper suppresses this observation. On the other hand, the observation window for the measurements with evolution times around 3 µs, distances just below 6 nm can be observed, with longer ones being suppressed heavily even by this 3.0D homogeneous background correction. Thus, though the finding of 6 nm sphere diameter might be intriguing to be identified with the particle diameter, it might as well be misleading. Furthermore, modulation depths are not increased too much, compared to the expected maximum modulation depth (see Table S 3), thus leaving no indication on which background correction one should use.

To summarize these considerations, there are significant intermolecular contributions to the form factors measured in nanoparticle samples. These intermolecular contributions may contain information on the particle size, but the data quality, especially the short evolution time, does not allow for reliable separation of inter- and intramolecular contributions in the distance distribution. Therefore, no conclusions can be drawn on the intermolecular contributions and we suppress those with the 2.4D homogeneous background correction used in the main manuscript.

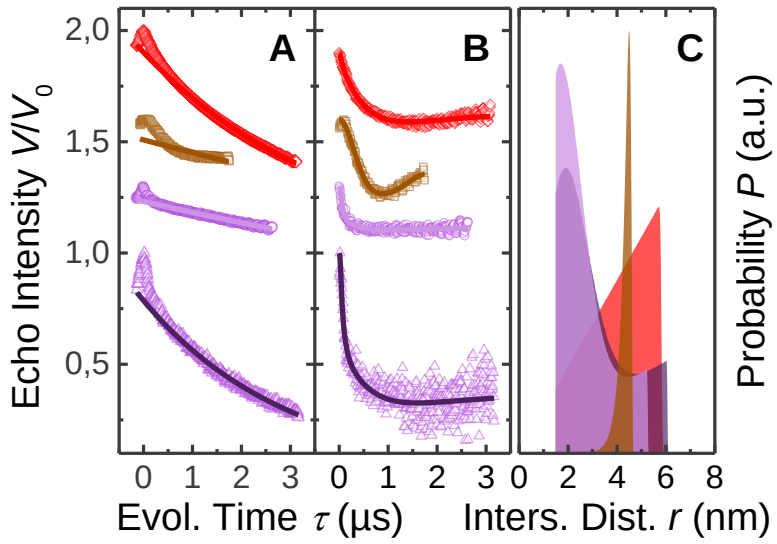

Figure S 5. A: Normalized DEER time traces recorded at 50 K in Q-band, with a 3.0D homogeneous background contribution of **SL-OPE$_{22}$** (red, diamonds). **DL-OPE$_5$** (brown, squares) and **DL-OPE$_{21}$** (dark violet, triangles) in particles with high **OPE$_{21}$**-content. Additionally, **DL-OPE$_{21}$** (light violet, circles) in particles with low **OPE$_{21}$**-content is shown. The colors follow the conventions from the main manuscript, only **SL-OPE$_{22}$** in red is new. B: Corresponding background corrected DEER form factors with model fits, all graphs are stretched by a factor of three for better visibility. C: Resulting distance distributions, only models included in DeerAnalysis were used: Sphere (red), WLC (brown), and Chechik_2 (violet). For all parameters see Table S 2.

Table S 2. Model fit parameters obtained from the *in-particle* DEER measurements shown in Figure S 5. The notation is as follows: $\langle r_1 \rangle$ is the mean distance of a Gaussian distance distribution, $s(r_1)$ its standard deviation, ds is a sphere diameter, and s(ds) its standard deviation, the total distance distribution is the weighted sum of both components, with the weighting factor p_1. The last three parameters are known from the main manuscript: L, the chain length, L_p, the persistence length, and σ, the standard deviation of an additional Gaussian broadening.

Sample	Model	$\langle r_1 \rangle$ nm	$s(r_1)$ nm	p_1 %	ds nm	s(ds) nm	L nm	L_p nm	σ nm
SL-OPE$_{22}$ in **PEG-OPE$_9$**-a Particles	Sphere	-	-	0	5.8	0.1	-	-	-
DL-OPE$_5$ in **PEG-OPE$_9$**-a Particles	WLC	-	-	-	-	-	4.7	9	0.0
DL-OPE$_{21}$ in **PEG-OPE$_9$**-a Particles	Sphere w/ Rice	1×10^{-3}	1.3	61	6.1	0.0	-	-	-
DL-OPE$_{21}$ in **PEG-OPE$_9$**-b Particles	Sphere w/ Rice	2×10^{-3}	1.2	70	5.3	0.0	-	-	-

Table S 3. Modulation depths of *in-particle* DEER measurements evaluated with a 3.0D background correction. On average, the modulation depth is 12±5 % normalized to pump pulse lengths.

Sample	Pump Pulse Length [ns]	Modulation Depth [%]	Norm. Mod. Depth [%]
DL-OPE$_5$ in **PEG-OPE$_9$**-a Particles	30	9	8
SL-OPE$_{22}$ in **PEG-OPE$_9$**-a Particles	40	12	15
DL-OPE$_{21}$ in **PEG-OPE$_9$**-a Particles	28	21	18
DL-OPE$_{21}$ in **PEG-OPE$_9$**-b Particles	34	7	7

SPIN CONCENTRATIONS AND DECAY OF THE HOMOGENEOUS BACKGROUND FUNCTIONS

Table S 4. Spin concentrations and densities of the homogeneous background functions of particle samples. The concentrations were obtained via integration of echo-detected field sweeps and referenced to **DL-OPE$_5$** in Toluene-d_8, where it was known from preparation. The density was determined similarly. It was set to 0.2 in DeerAnalysis with the data set of the aforementioned sample and then determined subsequently for all other samples.

Sample	Density [a.u.]	Spin Concentration [mM]
DL-OPE$_5$ in Toluene-d_8 Solution	0.2	0.2
DL-OPE$_5$ in **PEG-OPE$_9$**-a Particles	0.1	0.1
SL-OPE$_{22}$ in **PEG-OPE$_9$**-a Particles	0.8	0.6
DL-OPE$_{21}$ in **PEG-OPE$_9$**-a Particles	1.0	0.7 – 3.2*
DL-OPE$_{21}$ in **PEG-OPE$_9$**-b Particles	0.1	0.1

*: Unfortunately, for this sample the filling height is unknown as it is lost. Therefore the whole range of filling heights from 1 mm to 5 mm is assumed, leading to the range of concentrations indicated.

COMPARISON OF ALL DEER MEASUREMENTS OF DL-OPE$_{21}$

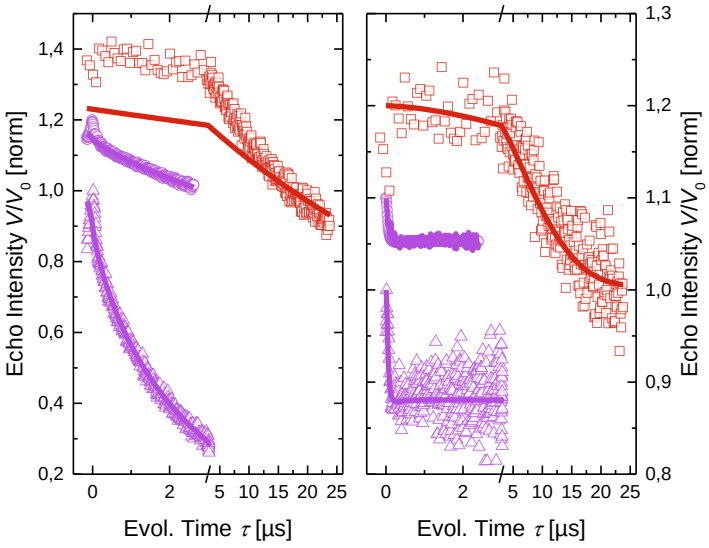

Figure S 6. Left: Normalized DEER traces recorded at 50 K in Q-band, with intermolecular background contribution of DL-OPE21 in particles (violet) with high (triangles) and low (circles) OPE21-content, and of DL-OPE21 in a solution of o-Terphenyl. The slopes of the intermolecular background contributions correspond to the concentrations of these samples. Right: Corresponding background corrected DEER form factors with a mutual fit of a distance distribution obtained from DEER and cw-ESR (cf. manuscript). Please note that the increment of the abscissa is increased after 3 µs in order to not compress or cut off the one or the other data.

COMPARISON OF THE BEST FIT DISTANCE DISTRIBUTIONS OBTAINED FROM CW AND FROM DEER FOR DL-OPE$_{21}$

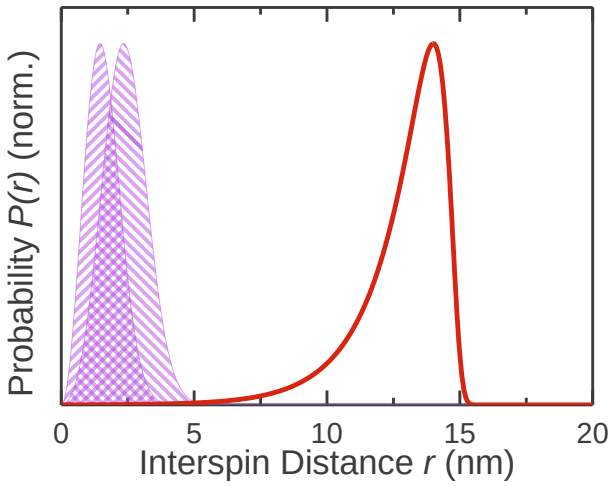

Figure S 7. Comparison of the experimental interspin distance distributions $P(r)$ of **DL-OPE$_{21}$** in particles obtained from the individual best fits to DEER (hatched downwards, longer distances) and cw-ESR (hatched upwards, shorter distances) data. The distance distribution shown in the main manuscript is an average of both distance distributions shown here. The extrapolated interspin distance distribution $P(r)$ of **DL-OPE$_{21}$** in solution is shown to allow for a complete picture.

ADDITIONAL CW-ESR SPECTRA

To prove dipolar broadening of cw-ESR spectra of **DL-OPE$_{21}$** inside nanoparticles indicating distances shorter than 1.5 nm[12], we compare these spectra to those of a singly labeled probe (**SL-OPE$_{22}$**) in similar particles as well as to those in larger particles (**PEG-OPE$_{21}$**, $D \approx 18$ nm). Compared to the control samples, the spectrum of the doubly labeled probe is significantly broader Concentration effects on the dipolar broadening can be excluded, since the spin concentration of the control samples was about the same or higher than the concentration of the broadened one (see Table S 5).

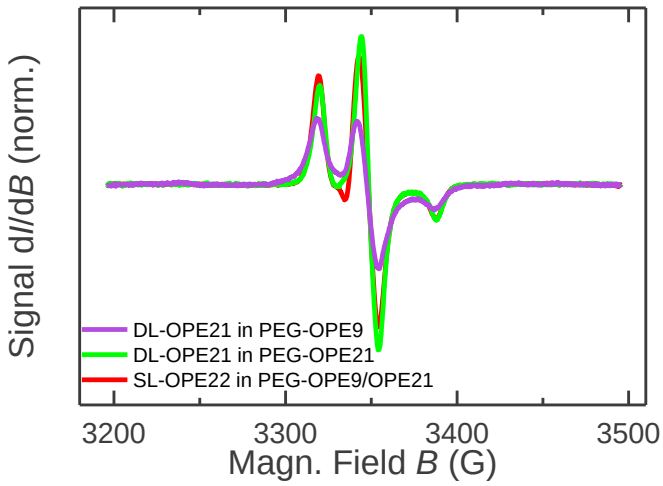

Figure S 8. Cw-EPR spectra of **DL-OPE$_{21}$** (purple) and of **SL-OPE$_{22}$** (red) in particles constituted by **PEG-OPE$_{9}$**, and of **DL-OPE$_{21}$** in particles of **PEG-OPE$_{21}$** (green) recorded at 120 K in X-band.

Table S 5. Concentrations of cw-ESR samples determined via the double integral and referenced to the concentration given in Table S 4 for **SL-OPE$_{22}$** in **PEG-OPE$_{9}$**-a particles.

Sample	Spin Concentration [mM]
SL-OPE$_{22}$ in **PEG-OPE$_{9}$**-a Particles	0.6
DL-OPE$_{21}$ in **PEG-OPE$_{9}$**-b Particles	0.3
DL-OPE$_{21}$ in **PEG-OPE$_{21}$**	0.3

REFERENCES

(1) Schütze, F.; Krumova, M.; Mecking, S. Size Control of Spherical and Anisotropic Fluorescent Polymer Nanoparticles via Precise Rigid Molecules. *Macromolecules* **2015**, *48*, 3900–3906.

(2) Chandler, D. Interfaces and the Driving Force of Hydrophobic Assembly. *Nature* **2005**, *437*, 640–647.

(3) Teraoka, I. *Polymer Solutions: An Introduction to Physical Properties*; 1st ed.; John Wiley & Sons: New York, NY, 2002.

(4) Li, I. T. S.; Walker, G. C. Interfacial Free Energy Governs Single Polystyrene Chain Collapse in Water and Aqueous Solutions. *J. Am. Chem. Soc.* **2010**, *132*, 6530–6540.

(5) Girifalco, L. A.; Good, R. J. A Theory for the Estimation of Surface and Interfacial Energies. I. Derivation and Application to Interfacial Tension. *J. Phys. Chem.* **1957**, *61*, 904–909.

(6) *CRC Handbook of Chemistry and Physics*; Lide, D. R., Ed.; 83rd ed.; CRC Press: Boca Raton, 2002.

(7) Maibaum, L.; Dinner, A. R.; Chandler, D. Micelle Formation and the Hydrophobic Effect†. *J. Phys. Chem. B* **2004**, *108*, 6778–6781.
(8) Godt, A.; Schulte, M.; Zimmermann, H.; Jeschke, G. How Flexible Are Poly(para-Phenyleneethynylene)s? *Angew. Chem. Int. Ed.* **2006**, *45*, 7560–7564.
(9) Jeschke, G.; Sajid, M.; Schulte, M.; Ramezanian, N.; Volkov, A.; Zimmermann, H.; Godt, A. Flexibility of Shape-Persistent Molecular Building Blocks Composed of P-Phenylene and Ethynylene Units. *J. Am. Chem. Soc.* **2010**, *132*, 10107–10117.
(10) Jeschke, G.; Chechik, V.; Ionita, P.; Godt, A.; Zimmermann, H.; Banham, J.; Timmel, C. R.; Hilger, D.; Jung, H. DeerAnalysis2006—a Comprehensive Software Package for Analyzing Pulsed ELDOR Data. *Appl. Magn. Reson.* **2006**, *30*, 473–498.
(11) Domingo Köhler, S.; Spitzbarth, M.; Diederichs, K.; Exner, T. E.; Drescher, M. A Short Note on the Analysis of Distance Measurements by Electron Paramagnetic Resonance. *J. Magn. Reson.* **2011**, *208*, 167–170.
(12) Banham, J. E.; Baker, C. M.; Ceola, S.; Day, I. J.; Grant, G. H.; Groenen, E. J. J.; Rodgers, C. T.; Jeschke, G.; Timmel, C. R. Distance Measurements in the Borderline Region of Applicability of CW EPR and DEER: A Model Study on a Homologous Series of Spin-Labelled Peptides. *J. Magn. Reson.* **2008**, *191*, 202–218.
(13) Ionita, P.; Volkov, A.; Jeschke, G.; Chechik, V. Lateral Diffusion of Thiol Ligands on the Surface of Au Nanoparticles: An Electron Paramagnetic Resonance Study. *Anal. Chem.* **2008**, *80*, 95–106.